# Core−Shell Nanoarchitectures: A Strategy To Improve the Efficiency of Luminescence Resonance Energy Transfer

**Cuihong Song,[†] Zhiqiang Ye,[‡] Guilan Wang,[‡] Jingli Yuan,[†,‡,*] and Yafeng Guan[†,*]**

[†]Department of Instrumentation and Analytical Chemistry, Dalian Institute of Chemical Physics, Chinese Academy of Sciences, Dalian 116023, China, and [‡]State Key Laboratory of Fine Chemicals, School of Chemistry, Dalian University of Technology, Dalian 116012, China

**ABSTRACT** The development of core−shell nanoparticles has shown a wide range of new applications in the fields of chemistry, bioscience, and materials science because of their improved physical and chemical properties over their single-component counterparts. In the present work, we took the core−shell nanoarchitectures as an example to research the luminescence resonance energy transfer (LRET) process between a luminescent $Tb^{3+}$ chelate, *N*,*N*,*N*$^1$,*N*$^1$-[4′-phenyl-2,2′:6′,2′-terpyridine-6,6′-diyl]bis(methylenenitrilo)tetrakis(acetate)-$Tb^{3+}$ (PTTA-$Tb^{3+}$), and an organic dye, 5-carboxytetramethylrhodamine (CTMR). PTTA-$Tb^{3+}$ and CTMR were chosen as the donor−acceptor pair of LRET in our model construction because of their effective spectral overlapping. The core−shell nanoparticles featuring a CTMR-$SiO_2$ core surrounded by a concentric PTTA-$Tb^{3+}$-$SiO_2$ shell were prepared using a reverse microemulsion method. These nanoparticles are spherical, uniform in size, and highly photostable. The results of LRET experiments show that the sensitized emission lifetime of the acceptor in the nanoparticles is significantly prolonged (~246 μs), which is attributed to the long emission lifetime of the $Tb^{3+}$ chelate donor. According to the results of the steady-state and time-resolved luminescence spectroscopy, an energy transfer efficiency of ~80% and a large Förster distance between the donor and the acceptor in the core−shell nanoparticles are calculated, respectively. The new core−shell nanoparticles with a high LRET efficiency and long Förster distance enable them to be promising optical probes for a variety of possible applications such as molecular imaging and multiplex signaling.

**KEYWORDS:** terbium chelate · tetramethylrhodamine · core−shell nanoparticle · luminescence resonance energy transfer

Fluorescence resonance energy transfer (FRET) technique is an important spectroscopic tool in bioanalysis,[1−4] especially in the detections of molecule binding events[5] and protein conformation change.[6] FRET occurs through the nonradiative dipole−dipole interactions between an excited donor molecule (D) and a proximal acceptor molecule (A) when the donor emission and the acceptor absorption are spectrally overlapped.[1] Although organic fluorophores have recently been demonstrated to be useful for the FRET studies even at the single-molecule level,[7] they have the limitations of broad emission spectra, small Stokes shifts, crosstalk between multicomponents, and poor photostability, thus restricting the more effective application of FRET technique. Over the past several years, luminescent lanthanide (mainly europium and terbium) chelates have frequently been used as donors in resonance energy transfer applications[2−4,8,9] because of their unusual spectral properties, including long luminescence lifetime, large Stokes shift, and sharply spiked emission bands (~10 nm full width at half-maximum).[10,11] These properties make the lanthanide-based resonance energy transfer, which is (more correctly) referred to as luminescence resonance energy transfer (LRET), have a number of technical advantages over the conventional FRET, although they rely on the same fundamental mechanism.[8]

In a LRET assay, the prolonged luminescence lifetime of the sensitized acceptor emission enables the measurement to be carried out with temporal and spectral separation from interfering background emission.[8,10] Temporal resolution can minimize the short-lived background noise caused by the directly excited acceptor emission, scattering lights, and possible autofluorescence of the sample. The background signal caused by the long lifetime donor emission can be effectively excluded with spectral resolution using a bandwidth emission filter having a narrow wavelength range where a lanthanide donor has a local emission minimum, but the acceptor emission is still sufficient for the measurement.[2,10,12] In addition, it has been reported that the LRET systems using lanthanide donors have larger Förster radii ($R_0$, the donor−acceptor distance where FRET is 50% efficient) up to 11 nm,[3,4] while the

*Address correspondence to jingliyuan@yahoo.com.cn, guanyafeng@dicp.ac.cn.

Received for review April 20, 2010 and accepted July 28, 2010.

**Published online August 3, 2010.** 10.1021/nn100820u

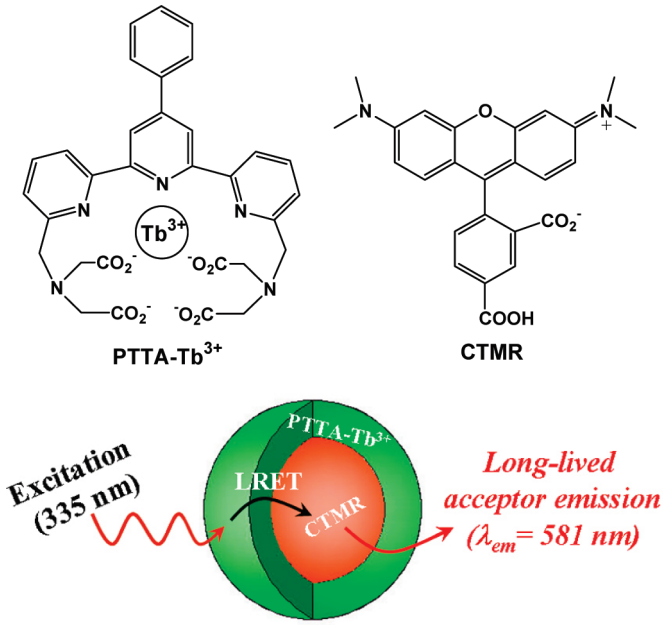


**Figure 1. Structures of PTTA-$Tb^{3+}$ chelate and CTMR (top), and general depiction of the CTMR core/PTTA-$Tb^{3+}$ shell silica nanoparticles showing the absorption of UV light (335 nm) by the PTTA-$Tb^{3+}$ shell (green emission) and subsequent LRET to the CTMR core (orange emission) (bottom).**

$R_0$ values of conventional donor–acceptor pairs are generally less than 6 nm,[13] which provides longer intermolecular distances and more efficient energy transfer for the LRET studies. These advantages make the lanthanide-based LRET assays useful for a number of diagnostic and biological applications.[4,10,13–21] However, it has to be mentioned that the lower photostability of conventional fluorophores used as the acceptors in LRET is still a problem because the LRET efficiency can be decreased by the irreversible photodegradation of the acceptor.[22]

It is expected that luminescent nanomaterials are one of the best choices for the study of energy transfer process, possessing the inherent characteristics for overcoming the limitations of conventional fluorophores.[22,23] In this regard, Tan *et al.*[23] have developed multicolor FRET silica nanoparticles by simultaneously incorporating three energy transfer fluorescent dyes into the silica matrix. Despite the considerable potential for multiplex bioanalysis and molecular imaging, these nanoparticles often suffer from quenching at high spatial density, counteracting their high dye loading. The development of core–shell nanostructures that display improved physical and chemical properties over their single-component counterparts has led to a wealth of new applications in the fields of chemistry, bioscience, and materials science.[22–25] Quite recently, Brodreau *et al.* reported the synthesis of multilayer core–shell nanoparticles displaying metal-enhanced FRET.[22] Their results demonstrated that the efficiency and distance of FRET could be significantly increased.

Luminescent lanthanide nanoparticles, with unique optical properties and better photo- and chemical stabilities,[25–27] have also been used as the energy donors for the LRET studies.[20,28–30] Since the energy transfer process strongly depends on the donor–acceptor distance,[8] it will be very helpful to conduct the well-defined core–shell nanostructures as a model to investigate the LRET process. However, to the best of our knowledge, there has been no report on the LRET from the lanthanide chelates to organic dyes in the core–shell nanoparticles. A fundamental question that we are attempting to address in this work is how the energy transfer occurs and whether the LRET efficiency is improved in the core–shell nanoparticles. We chose a luminescent $Tb^{3+}$ chelate, *N*,*N*,*N*$^1$,*N*$^1$-[4′-phenyl-2,2′:6′,2′-terpyridine-6,6′-diyl]bis(methylenenitrilo)tetrakis(acetate)-$Tb^{3+}$ (PTTA-$Tb^{3+}$), as the energy donor and an organic dye, 5-carboxytetramethylrhodamine (CTMR), as the energy acceptor because of their well-documented photophysical properties and their good overlapping of absorption and emission bands.[12] After the well-dispersed spherical CTMR core/PTTA-$Tb^{3+}$ shell silica nanoparticles were prepared by covalent linking CTMR and PTTA-$Tb^{3+}$ into the silica matrix using a reverse microemulsion method,[31–33] the LRET from the PTTA-$Tb^{3+}$ shell to the CTMR core was studied by using steady-state and time-resolved luminescence spectroscopy methods. The results of our study demonstrate that the efficiency and distance of LRET can be significantly increased by covalently linking the donor–acceptor pair into the core–shell silica nanoparticles, which opens up a new perspective for the design of silica-based multifunctional nanostructures. Figure 1 shows the structures of PTTA-$Tb^{3+}$, CTMR, and the core–shell nanoparticles.

## RESULTS AND DISCUSSION

**Preparation and Characterization of the Core–Shell Silica Nanoparticles.** In this work, PTTA-$Tb^{3+}$ and CTMR were employed for the preparation of silica-based core–shell nanoparticles for LRET studies because they have a good spectral overlapping and can be covalently linked into the silica matrix. Figure 2 shows the emission spectrum of PTTA-$Tb^{3+}$ and the excitation and emission spectra of the CTMR. The emission peaks of PTTA-$Tb^{3+}$ at 487 and 541 nm are well overlapped with the excitation spectrum of CTMR, satisfying the prerequisite for efficient LRET. It is also notable that the emission intensity of PTTA-$Tb^{3+}$ is nearly silent around 565 nm (~100-fold lower than that of its maximum at 541 nm), where CTMR is at ~90% of its emission maximum (577 nm). These spectral characteristics of PTTA-$Tb^{3+}$ and CTMR enable the effective elimination of the direct emission of CTMR when the sensitized long-lived emission of CTMR at 565 nm in the LRET system is measured with time-resolved detection mode, which allows a high signal/background ratio to be obtained when PTTA-$Tb^{3+}$

and CTMR are used as the donor−acceptor pair for the LRET measurement.

To investigate the LRET performance of PTTA-$Tb^{3+}$−CTMR donor−acceptor pair in nanostructures, the CTMR core/PTTA-$Tb^{3+}$ shell silica nanoparticles were synthesized using a W/O micromulsion method by a two-step procedure involving the preparation of the CTMR−silica core and the *in situ* postcoating of the PTTA-$Tb^{3+}$−silica shell. After the EDC/NHS-activated CTMR and PTTA-$Tb^{3+}$ were covalently conjugated to APS,[34,35] the CTMR−silica cores were first prepared by the hydrolysis and copolymerization of the APS−CTMR conjugate and TEOS in the W/O microemulsion. The *in situ* postcoating of the CTMR−silica cores with APS−PTTA-$Tb^{3+}$ conjugate, TEOS, and APS in the microemulsion enabled the formation of a PTTA-$Tb^{3+}$−silica shell surrounding the CTMR−silica cores, yielding the CTMR core/PTTA-$Tb^{3+}$ shell silica nanoparticles. The use of APS in the postcoating process allowed the amino groups to be directly introduced onto the nanoparticles' surface, to provide an additional function for the further application of the nanoparticles.

For comparison, the acceptor-only CTMR@$SiO_2$ nanoparticles and donor-only PTTA-$Tb^{3+}$@$SiO_2$ nanoparticles were also synthesized under the same synthetic conditions (for details, see Synthesis of the Core−Shell Nanoparticles in Materials and Methods). It has been reported that the luminescence lifetime of PTTA-$Tb^{3+}$-doped silica nanoparticles is remarkably longer than that of the free PTTA-$Tb^{3+}$ chelate.[35] The results of time-resolved measurements showed that, in aqueous solution, the luminescence lifetime for the PTTA-$Tb^{3+}$@$SiO_2$ nanoparticles was 1.21 ± 0.02 ms (the decay curve is shown in Figure 6a), while that for free PTTA-$Tb^{3+}$ was only 0.45 ms,[36] indicating that the PTTA-$Tb^{3+}$ donor was effectively protected from the luminescence quenching by the silica matrix. Figure 3 gives the bright-field and luminescence (under a 365 nm UV lamp) photographs of the three kinds of nanoparticles dispersed in the aqueous buffer (in Figure 3a, the reflectance of the black background seems to be occurring, but it has no effect on the luminescence observation). It was interesting to see that a much stronger pink emission color was observed from the solution of CTMR-PTTA-$Tb^{3+}$@$SiO_2$ nanoparticles, even though the luminescence of CTMR@$SiO_2$ nanoparticle solution is very weak under irradiation of the 365 nm UV lamp. This phenomenon can be explained by the fact that the weak luminescence of CTMR@$SiO_2$ nanoparticles is due to the weak absorption of CTMR at 365 nm. While in the core−shell CTMR-PTTA-$Tb^{3+}$@$SiO_2$ nanoparticles, due to the absorption of PTTA-$Tb^{3+}$ at 365 nm and the LRET from the $Tb^{3+}$ chelate to CTMR, the luminescence of CTMR is remarkably enhanced. This result also demonstrated the existence of the efficient energy transfer from the PTTA-$Tb^{3+}$ shell to the CTMR core in the CTMR-PTTA-$Tb^{3+}$@$SiO_2$ nanoparticles.

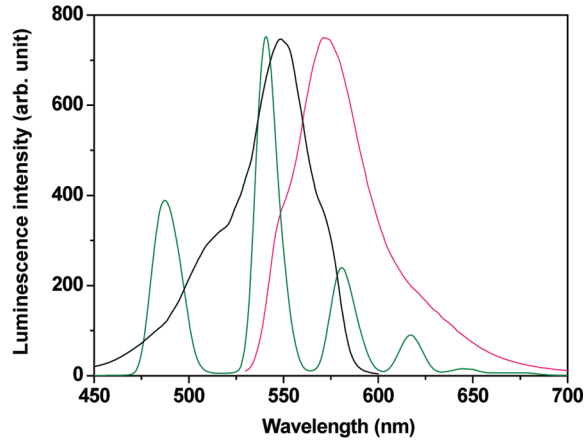


**Figure 2. Emission spectrum of PTTA-$Tb^{3+}$ chelate ($\lambda_{ex}$ = 335 nm, green line) and the excitation ($\lambda_{em}$ = 577 nm, black line) and emission ($\lambda_{ex}$ = 557 nm, pink line) spectra of CTMR.**

High-resolution transmission electron microscopy (HRTEM) was used for the characterization of the nanoparticles. As shown in Figure 4, different from the single-layer structure of the CTMR@$SiO_2$ nanoparticles, the PTTA-$Tb^{3+}$@$SiO_2$ and the CTMR-PTTA-$Tb^{3+}$@$SiO_2$ nanoparticles show that the core−shell structures, despite the shell thickness, are formed. The formation of the core−shell structure is attributed to the two-step preparation method (see the section of Materials and Methods). The mean particle diameters (±SD) of the CTMR@$SiO_2$ nanoparticles and the PTTA-$Tb^{3+}$@$SiO_2$ nanoparticles are 51 ± 2 and 54 ± 3 nm, respectively, while that of the core−shell CTMR-PTTA-$Tb^{3+}$@$SiO_2$ nanoparticles is 69 ± 2 nm. The observed increase in size of the CTMR-PTTA-$Tb^{3+}$@$SiO_2$ nanoparticles compared with that of the CTMR@$SiO_2$ nanoparticles is attributed to the presence of the PTTA-$Tb^{3+}$−silica shell around the CTMR−silica core. The smaller size of the PTTA-$Tb^{3+}$@$SiO_2$ nanoparticles compared with that of the CTMR-PTTA-$Tb^{3+}$@$SiO_2$ nanoparticles is due to the different water/oil ratios in the W/O micromulsions because 100 μL of water was used instead of 100 μL of the APS−CTMR conjugate for the synthesis of the PTTA-$Tb^{3+}$@$SiO_2$ nanoparticles. From the difference in particle sizes between the CTMR@$SiO_2$ and the CTMR-PTTA-$Tb^{3+}$@$SiO_2$ nanoparticles, the thickness of the PTTA-$Tb^{3+}$−silica shell in the CTMR-PTTA-$Tb^{3+}$@$SiO_2$ nanoparticles is evaluated to be ~9 nm. It is known that

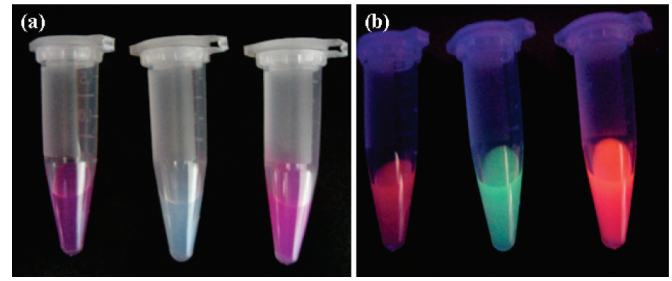


**Figure 3. (a) Bright-field and (b) luminescence (under a 365 nm UV lamp) photographs of colloidal solutions of CTMR@$SiO_2$ (left), PTTA-$Tb^{3+}$@$SiO_2$ (middle), and CTMR-PTTA-$Tb^{3+}$@$SiO_2$ (right) nanoparticles.**

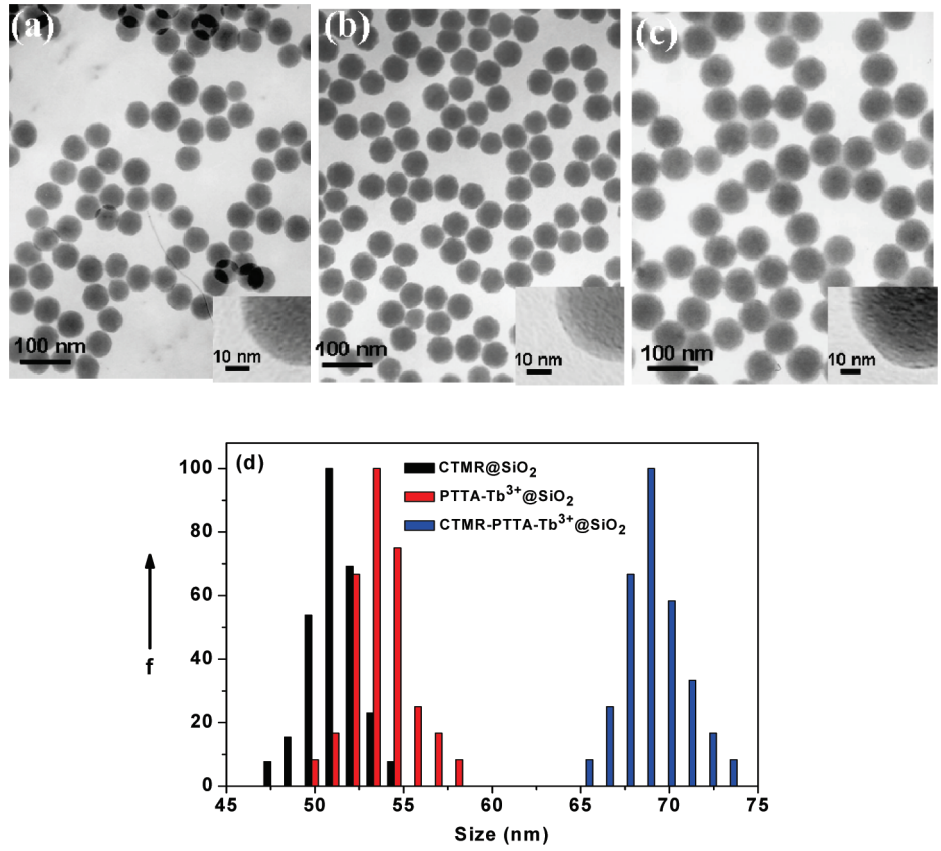


**Figure 4. TEM images of the CTMR@$SiO_2$ (a), the PTTA-$Tb^{3+}$@$SiO_2$ (b), and the core−shell CTMR-PTTA-$Tb^{3+}$@$SiO_2$ (c) nanoparticles. (d) Particle size distribution histograms of the three kinds of nanoparticles.**

the LRET efficiency depends on the separated distance of the donor and acceptor molecules (proportional to $R^{-6}$), and LRET with a lanthanide donor typically occurs over distances up to 11 nm.[3,4] Therefore, the LRET from the PTTA-$Tb^{3+}$−silica shell to the CTMR−silica core is possible because the distance between the donor (PTTA-$Tb^{3+}$) and the acceptor (CTMR) is within the Förster distance.

**LRET of the Core−Shell CTMR-PTTA-$Tb^{3+}$@$SiO_2$ Nanoparticles.** To investigate the LRET process of the core−shell CTMR-PTTA-$Tb^{3+}$@$SiO_2$ nanoparticles, the luminescence spectra of the nanoparticles were measured with both the steady-state mode and the time-resolved mode. Figure 5 shows the steady-state emission spectra of the CTMR@$SiO_2$ and the CTMR-PTTA-$Tb^{3+}$@$SiO_2$ nanoparticles dispersed in the aqueous buffer. The luminescence at 581 nm of the CTMR-PTTA-$Tb^{3+}$@$SiO_2$ nanoparticles is ~13-fold higher than that of the CTMR@$SiO_2$ nanoparticles, while only a weak donor emission at 541 nm is observed. It is therefore reasonable to assume that the high acceptor/donor emission ratio observed in the spectrum of the core−shell nanoparticles results from a very efficient LRET from the donor shell to the acceptor core.

It has been known that the luminescence lifetime of the sensitized acceptor emission in the LRET systems using luminescent lanthanide chelates as the donors can be significantly prolonged (over tens to hundreds of microseconds), which enables the measurement to be carried out with time-resolved mode to eliminate the interferences from the assay matrix and the direct short-lived acceptor emission. Therefore, the LRET of the core−shell CTMR-PTTA-$Tb^{3+}$@$SiO_2$ nanoparticles was further confirmed by the time-resolved luminescence measurement. In this work, the time-resolved emission spectra of the new nanoparticles were measured with a gate time of 0.40 ms and a series of delay times (from 0.05 to1.0 ms). By using this mode, the direct emission of CTMR (several nanoseconds of emission lifetime) was completely eliminated. Figure 6a,b shows the time-resolved emission spectra of the donor-only PTTA-$Tb^{3+}$@$SiO_2$ nanoparticles and the core−shell CTMR-PTTA-$Tb^{3+}$@$SiO_2$ nanoparticles dispersed in the aqueous buffer at different delay times. It can be observed that the donor-only PTTA-$Tb^{3+}$@$SiO_2$ nanoparticles show a typical $Tb^{3+}$ emission pattern with a main emission peak at 541 nm ($^5D_4 \rightarrow {}^7F_5$) and several side peaks centered at 486, 581, and 617 nm. The inset in Figure 6a shows the emission intensity change of the PTTA-$Tb^{3+}$@$SiO_2$ nanoparticles at 541 nm against different delay times. The correlation between the natural logarithm of the emission intensity of the nanoparticles and the delay time shows a good linearity that can be accurately fitted to the equation $y = 6.389 - 0.829x$ ($R^2 = 0.998$). This result demonstrates that

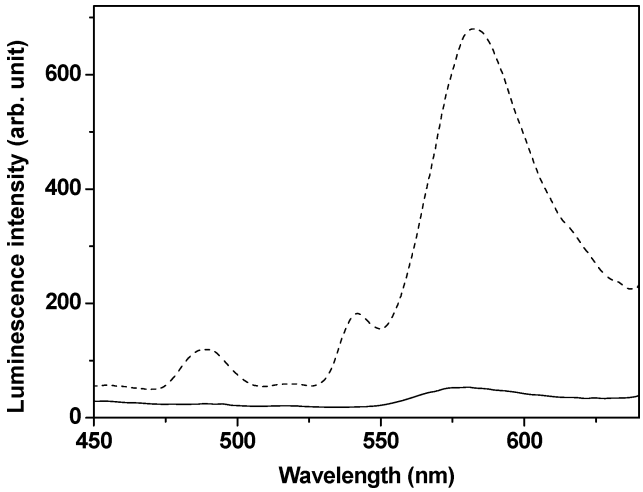


**Figure 5. Steady-state emission spectra ($\lambda_{ex}$ = 335 nm) of the CTMR@$SiO_2$ nanoparticles (100 mg/L, solid line) and the core−shell CTMR-PTTA-$Tb^{3+}$@$SiO_2$ nanoparticles (100 mg/L, dashed line).**

the luminescence of the PTTA-$Tb^{3+}$@$SiO_2$ nanoparticles has a single exponential decay with a lifetime of 1.21 ms. Compared with the spectra of the PTTA-$Tb^{3+}$@$SiO_2$ nanoparticles, although the emission peak position is unchanged, the emission peak breadth and intensity of the CTMR-PTTA-$Tb^{3+}$@$SiO_2$ nanoparticles at 581 nm are distinctly increased (Figure 6b), which can be considered to be attributed to the sensitized delayed emission of the acceptor (CTMR) in the nanoparticles. To further confirm the occurrence of LRET only when the donor−acceptor pair is in very close proximity, the emission spectra of PTTA-$Tb^{3+}$@$SiO_2$ nanoparticles with steady-state and time-resolved modes in the presence of free CTMR were also determined. As shown in Figure 6c, in the presence of free CTMR, the emission intensity of the PTTA-$Tb^{3+}$@$SiO_2$ nanoparticles at 581 nm in the steady-state spectrum was significantly increased and the spectrum pattern was quite similar to that of CTMR-PTTA-$Tb^{3+}$@$SiO_2$ nanoparticles (dashed line in Figure 5). However, when time-resolved mode was used, the emission of CTMR disappeared, and the spectrum was recovered nearly the spectrum of the PTTA-$Tb^{3+}$@$SiO_2$ nanoparticles (weakly affected by the long-distance LRET). This result demonstrates that the efficient LRET occurs

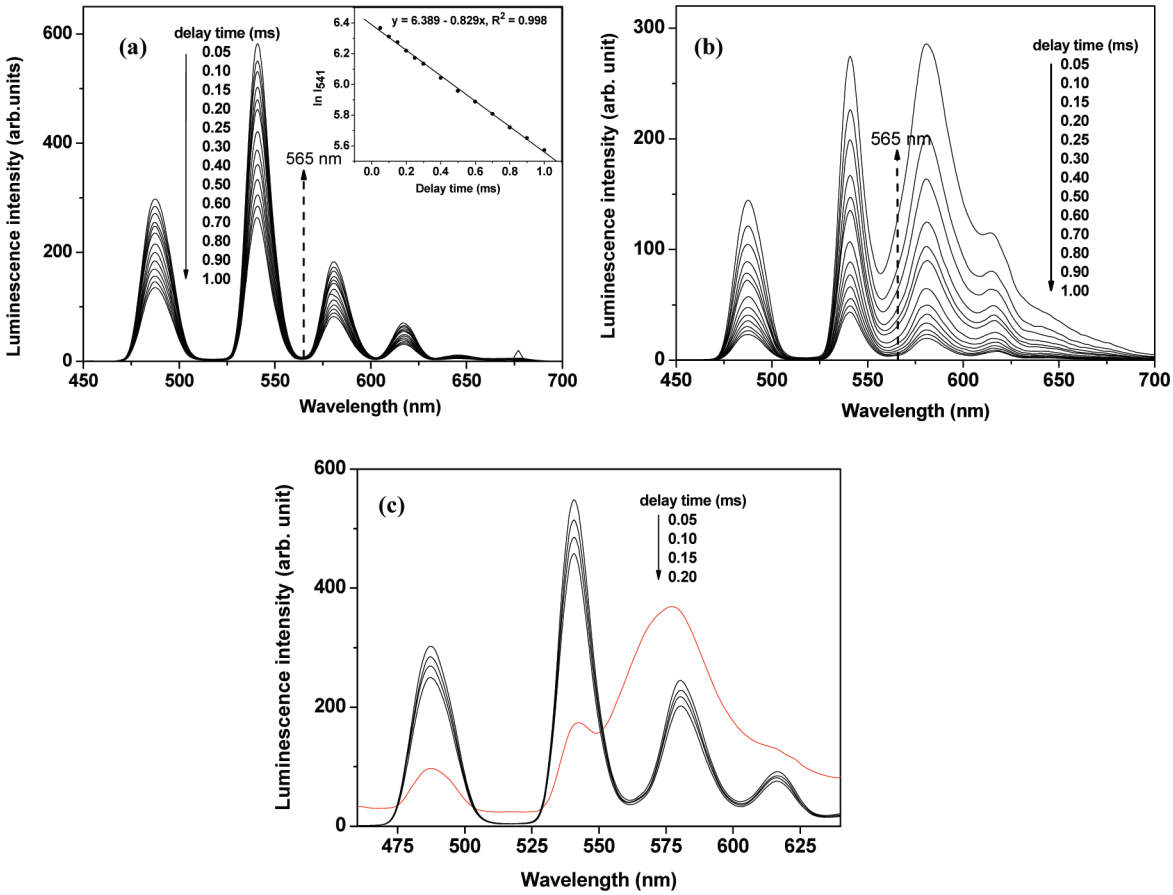


**Figure 6. (a) Time-resolved emission spectra of the donor-only PTTA-$Tb^{3+}$@$SiO_2$ nanoparticles (100 mg/L; the inset shows the correlation between the natural logarithm of luminescence intensity of the nanoparticles at 541 nm and delay time) and (b) the core−shell CTMR-PTTA-$Tb^{3+}$@$SiO_2$ nanoparticles (100 mg/L) at different delay times. (c) Steady-state (red line) and time-resolved (black lines at different delay times) emission spectra of the donor-only PTTA-$Tb^{3+}$@$SiO_2$ nanoparticles (100 mg/L) in the presence of free CTMR (1.0 μM).**

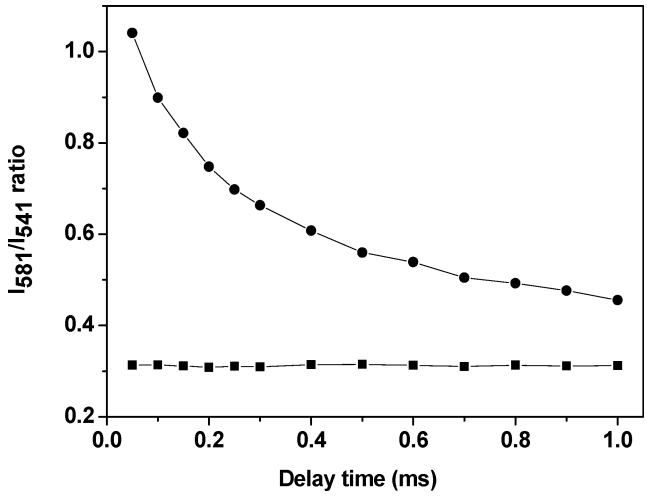


**Figure 7. Emission intensity ratio of $I_{581}/I_{541}$ ($\lambda_{ex}$ = 335 nm) of the nanoparticles (100 mg/L) as a function of delay time (square, PTTA-$Tb^{3+}$@$SiO_2$ nanoparticles; circle, CTMR-PTTA-$Tb^{3+}$@$SiO_2$ nanoparticles).**

only when the donor−acceptor pair is in a very short distance.

Figure 7 shows the emission intensity ratio change of 581 to 541 nm ($I_{581}/I_{541}$) of the PTTA-$Tb^{3+}$@$SiO_2$ nanoparticles and the core−shell CTMR-PTTA-$Tb^{3+}$@$SiO_2$ nanoparticles as a function of delay time. It is notable that the $I_{581}/I_{541}$ ratio obtained from the spectra of the CTMR-PTTA-$Tb^{3+}$@$SiO_2$ nanoparticles is higher than that obtained from the spectra of the PTTA-$Tb^{3+}$@$SiO_2$ nanoparticles in all cases (delay time varied from 0.05 to 1.0 ms). With the increase of delay time from 0.05 to 1.0 ms, the $I_{581}/I_{541}$ ratios of the PTTA-$Tb^{3+}$@$SiO_2$ nanoparticles are almost unchanged (~0.31), while those of the CTMR-PTTA-$Tb^{3+}$@$SiO_2$ nanoparticles are decreased from 1.04 to 0.46. The above results indicate that the sensitized emission lifetime of CTMR is significantly delayed (but has a faster decay compared with the PTTA-$Tb^{3+}$ donor), and the energy transfer from the $Tb^{3+}$ chelate to CTMR is quite efficient in the core−shell nanoparticles.

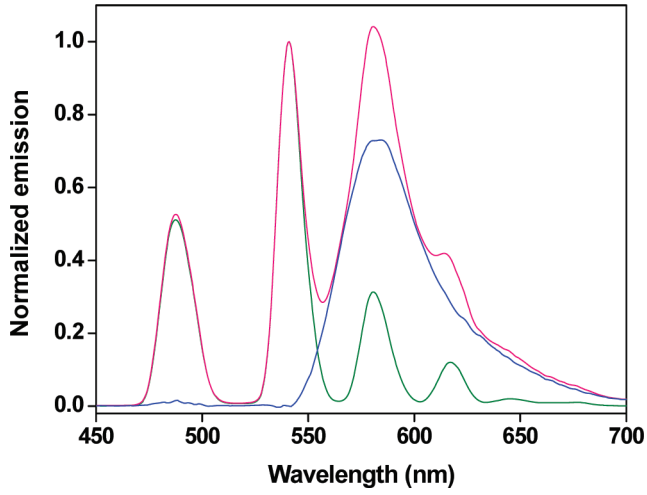


**Figure 8. Normalized time-resolved emission spectra ($\lambda_{ex}$ = 335 nm, delay time = 50 μs) of the donor-only PTTA-$Tb^{3+}$@$SiO_2$ nanoparticles (green line) and the donor−acceptor CTMR-PTTA-$Tb^{3+}$@$SiO_2$ nanoparticles (pink line), and the difference spectrum (blue line) by subtracting the donor emission from the donor−acceptor emission.**

Using the Selvin's method,[12] the sensitized acceptor emission was isolated from the donor emission. As shown in Figure 8, after the emission curves of the donor-only PTTA-$Tb^{3+}$@$SiO_2$ nanoparticles (green line) and the donor−acceptor CTMR-PTTA-$Tb^{3+}$@$SiO_2$ nanoparticles (pink line) were normalized at 541 nm, the donor emission was subtracted at all wavelengths from the donor−acceptor emission, leaving the difference emission which was attributed to the sensitized emission of the acceptor (blue line). As expected, the shape of the difference emission is nearly the same as that of the acceptor-only CTMR@$SiO_2$ nanoparticles (Figure 5, solid line). Thus the LRET efficiency ($E$) from the $Tb^{3+}$ chelate to CTMR in the core−shell nanoparticles was approximately calculated to be 81% by using the areas under the corrected sensitized emission curve ($f_A$) and the donor emission curve ($f_D$) and a quantum yield of tetramethylrhodamine (TMR, $q_A$ = 0.174)[12] with the equation $E = (f_A/q_A)/(f_A/q_A + f_D)$.[12]

In a LRET system, the energy transfer efficiency ($E$) can also be determined by measuring the lifetimes of the donor's emission in the absence of acceptor ($\tau_D$) and the sensitized emission of acceptor ($\tau_{AD}$) using the equation $E = 1 - (\tau_{AD}/\tau_D)$.[8] In this work, the PTTA-$Tb^{3+}$ donor has a very weak emission at 565 nm, where the sensitized CTMR emission is significantly strong, and the signal/background ratio at 565 nm is approximately 32:1 calculated by dividing the signal of donor−acceptor pair and the signal of donor-only at 565 nm[12] (Figure 8). Thus, the luminescence decay curve of the sensitized acceptor emission was determined by monitoring the intensity change at 565 nm. As shown in Figure 9, the decay curve of the sensitized acceptor emission shows a double exponential correlation that can be expressed as $y = 63.5\%\exp(-t/0.012) + 39.1\%\exp(-t/0.246) + 0.088$ ($R^2$ = 0.998). The short lifetime of 12 ± 1.5 μs corresponds to the luminescence from a detector artifact[12] or a donor−acceptor pair at a very short distance, and the long lifetime of 246 ± 19 μs is attributed to the energy transfer from the $Tb^{3+}$ chelate donor to the CTMR acceptor in the nanoparticles. Consequently, using $\tau_{AD}$ = 246 μs and $\tau_D$ = 1.21 ms, the LRET efficiency for the core−shell CTMR-PTTA-$Tb^{3+}$@$SiO_2$ nanoparticles was calculated to be 80 ± 2% using the equation $E = 1 - (\tau_{AD}/\tau_D)$, which is corresponds well with the result calculated from the areas of the corrected sensitized emission curves. Therefore, it is reasonable to suggest that the enhancement of LRET efficiency is achieved by employing the novel core−shell nanostructure where the acceptor and donor are covalently linked into the core and shell, respectively.

In addition, as observed in the TEM images, the core−shell CTMR-PTTA-$Tb^{3+}$@$SiO_2$ nanoparticles are

quite monodispersed and the CTMR acceptor is located in the center of the PTTA-$Tb^{3+}$ donor shell. Thus the average donor−acceptor distance ($R$) can be considered to be a constant. However, to determine the exact average $R$ of LRET in the nanoparticles is difficult. To roughly estimate the $R_0$ value in the core−shell nanoparticles, we assume that the average $R$ is in the range of 4.5 to 9 nm (from half to full of the shell thickness). On the basis of this hypothesis, the Förster radius $R_0$ of the core−shell CTMR-PTTA-$Tb^{3+}$@$SiO_2$ nanoparticles was calculated to be in the range of 57 to 113 Å using the equation $R_0 = R \times [E/(1 - E)]^{1/6}$.[8] The effective enhancement of LRET efficiency and large Förster distance of the core−shell CTMR-PTTA-$Tb^{3+}$@$SiO_2$ nanoparticles can be considered to be attributed to the effective energy transfer from the excited PTTA-$Tb^{3+}$ donor in the shell to the CTMR acceptor in the core. It is also worth considering that the luminescent core−shell nanoparticles have clear advantages over the uncoated materials in terms of enhanced luminescence and photostability.[22,37,38] Moreover, since the donor and the acceptor molecules are both covalently attached into the core−shell silica nanoparticles, the dye-leaking problem is well-resolved, which favors the long-term employment of the nanoparticles for the LRET studies. However, because the average donor−acceptor distance was fixed in the present work, the dependence of the LRET efficiency on the donor−acceptor distance was not determined. It shall be interesting to conduct the studies on the distance-dependent LRET efficiency between various lanthanide donors and suited acceptors in the core−shell nanostructures.

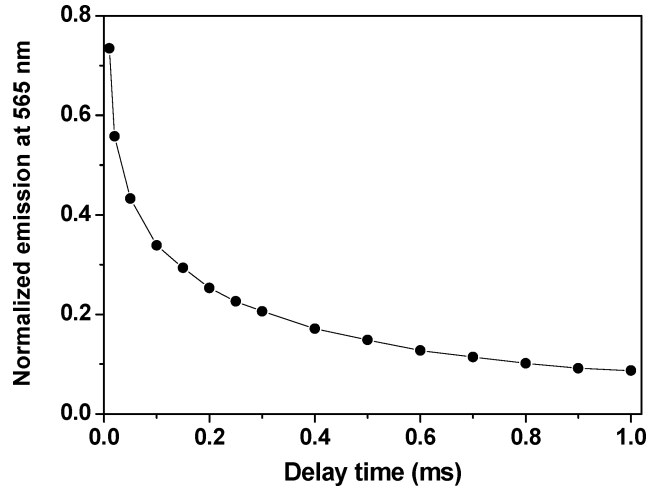


**Figure 9. Decay curve of the sensitized acceptor emission at 565 nm.**

## CONCLUSIONS

In conclusion, a core−shell nanoparticle-based strategy for improving the LRET efficiency was presented in this work. Using a versatile, simple, and reproducible method, the luminescent dye covalently linked silica nanoparticles featuring an organic acceptor (CTMR) core surrounded by a concentric lanthanide chelate donor (PTTA-$Tb^{3+}$) shell were prepared. The as-prepared nanoparticles are monodisperse, spherical, uniform in size, and well-dispersed in water. The LRET experiments of the new nanoparticles were conducted with steady-state and time-resolved luminescence spectroscopy methods. Thanks to the long lifetime and sharply spiked emission of the lanthanide donor, the sensitized emission of the acceptor can be measured with temporal and spectral separation from the interfering background emissions. More importantly, the increased Förster distance and efficiency of LRET in the core−shell nanoparticles and their enhanced photostability allow them to be promising optical probes for a variety of possible applications. It is also expected that the core−shell nanoparticle model presented in this work can be further extended to two or more LRET pairs to generate various multicolor and multilayer core−shell nanoparticles for the multiplexed detections.

## MATERIALS AND METHODS

**Materials and Instrumentation.** The ligand PTTA was synthesized according to a reported method.[36] Triton X-100, (3-aminopropyl)triethoxylsilane (APS), tetraethyl orthosilicate (TEOS), *N*-hydroxysuccinimide (NHS), and 1-ethyl-3-(3-dimethylaminopropyl)carbodiimide hydrochloride (EDC) were purchased from Acros Organic. Unless otherwise stated, all chemicals were purchased from commercial sources and used without further purification.

Luminescence spectra and lifetimes were measured on a Perkin-Elmer LS 50B luminescence spectrometer with the conditions of excitation slit, 10 nm; emission slit, 5 nm. UV−vis absorption spectra were measured on a Perkin-Elmer Lambda 35 UV−vis spectrometer. All spectra were recorded at room temperature. The shape and size of the nanoparticles were measured on a JEOL JEM-2000EX transmission electron microscope.

**Synthesis of APS−CTMR and APS−PTTA-$Tb^{3+}$ Conjugates.** According to the reported methods,[34,35] the APS−CTMR and APS−PTTA-$Tb^{3+}$ conjugates were synthesized as follows.

(i) Synthesis of APS−CTMR conjugate: To 240 μL of anhydrous ethanol solution containing 3.7 mg of EDC and 1.2 mg of NHS was added 60 μL of 0.05 M sodium carbonate buffer of pH 9.5 containing 3.9 mg of CTMR. The mixture was agitated for 30 min, and then 5.0 μL of APS was added with stirring. The reaction was allowed to continue for another 2 h. The obtained solution containing the APS−CTMR conjugate was used in the next step without further manipulation.

(ii) Synthesis of APS−PTTA-$Tb^{3+}$ conjugate: To 200 μL of anhydrous ethanol solution containing 9.0 mg of EDC and 2.8 mg of NHS was added 50 μL of 0.05 M sodium carbonate buffer of pH 9.5 containing 3.8 mg of PTTA · $1.5H_2O$. The mixture was agitated for 30 min, followed by the addition of 5.0 μL of APS. The reaction was kept for another 2 h. Then 50 μL of aqueous solution containing 2.3 mg of $TbCl_3 \cdot 6H_2O$ was added, and the mixture was further stirred for 15 min. The obtained solution containing the APS−PTTA-$Tb^{3+}$ conjugate was used in the next step without further manipulation. ESI-MS for APS−PTTA (base peak): positive mode, $m/z$ 734.2 (100%) $[M - 2OC_2H_5 - H + Na]^+$; negative mode, $m/z$ 689.3 (100%) $[M - 3OC_2H_5 - H + Na]^-$. No molecular ion peaks of free PTTA and APS−PTTA were observed.

**Synthesis of the Core−Shell Nanoparticles.** The CTMR core/PTTA-$Tb^{3+}$ shell silica nanoparticles were prepared in a water-in-oil (W/O) reverse microemulsion with the following procedure. To a solution consisting of 1.77 g of Triton X-100, 1.6 mL of

*n*-octanol, and 7.5 mL of cyclohexane were added 100 μL of APS−CTMR conjugate solution and 300 μL of water to obtain a W/O microemulsion. After the solution was stirred for 30 min, 100 μL of TEOS was added. The polymerization reaction was initiated by adding 60 μL of concentrated aqueous ammonia. After stirring for 24 h, 100 μL of APS−PTTA-$Tb^{3+}$ conjugate solution was added. The solution was stirred for 30 min, and then 100 μL of TEOS and 5 μL of APS were added. The mixture was stirred for another 36 h. The nanoparticles were isolated from the microemulsion by adding 10 mL of acetone, followed by centrifuging and washing with ethanol and water several times to remove the surfactant and unreacted materials. For comparison, the acceptor-only CTMR@$SiO_2$ nanoparticles (CTMR−silica cores, no postcoating step of APS−PTTA-$Tb^{3+}$ conjugate) and donor-only PTTA-$Tb^{3+}$@$SiO_2$ nanoparticles (the pure silica core was synthesized using 100 μL of water instead of 100 μL of APS−CTMR conjugate, and then the core was postcoated with PTTA-$Tb^{3+}$−silica shell) were also synthesized under the same synthetic conditions.

**LRET Measurements.** All of the measurements were carried out in 0.05 M Tris-HCl buffer of pH 7.4 with the same concentration of the nanoparticles (100 mg/L). The spectra of LRET were measured with two modes.[10] One is steady-state luminescence mode, and another is time-resolved luminescence mode. The time-resolved luminescence spectra were recorded with a gate time of 400 μs and different delay times after the pulse excitation. In the case of time-resolved mode, only the luminescence of long-lived species was detected, and that of short-lived species was eliminated. The luminescence decay curves were measured using a previous method[10] by recording the sensitized acceptor emission at 565 nm with a gate time of 400 μs and different delay times. The LRET efficiency (*E*) was determined by using two methods: (1) *E* was determined and calculated using the equation $E = (f_A/q_A)/(f_A/q_A + f_D)$,[12] where $f_A$ and $f_D$ are the areas under the sensitized emission curve of acceptor and the donor emission curve, respectively, and $q_A$ is the luminescence quantum yield of the acceptor. (2) *E* was determined and calculated using the equation $E = 1 - (\tau_{AD}/\tau_D)$,[8] where $\tau_D$ is the donor's emission lifetime in the absence of acceptor, and $\tau_{AD}$ is the lifetime of the sensitized emission of acceptor.

*Acknowledgment.* Financial support from the National Natural Science Foundation of China (Nos. 20835001, 20975017) and the Specialized Research Fund for the Doctoral Program of Higher Education of China (No. 200801410003) is gratefully acknowledged.

## REFERENCES AND NOTES

1. Lakowicz, J. R. *Principles of Fluorescence Spectroscopy*, 2nd ed.; Kluwer /Plenum: New York, 1999.
2. Selvin, P. R.; Rana, T. M.; Hearst, J. E. Luminescence Resonance Energy Transfer. *J. Am. Chem. Soc.* **1994**, *116*, 6029–6030.
3. Sapsford, K. E.; Berti, L.; Medintz, I. L. Materials for Fluorescence Resonance Energy Transfer Analysis: Beyond Traditional Donor−Acceptor Combinations. *Angew. Chem., Int. Ed.* **2006**, *45*, 4562–4588.
4. Geissler, D.; Charbonnière, L. J.; Ziessel, R. F.; Butlin, N. G.; Löhmannsröben, H. G.; Hildebrandt, N. Quantum Dot Biosensors for Ultrasensitive Multiplexed Diagnostics. *Angew. Chem., Int. Ed.* **2010**, *49*, 1396–1401.
5. Peng, H.; Zhang, L.; Kjällman, T. H. M.; Soeller, C.; Travas-Sejdic, J. DNA Hybridization Detection with Blue Luminescent Quantum Dots and Dye-Labeled Single-Stranded DNA. *J. Am. Chem. Soc.* **2007**, *129*, 3048–3049.
6. Lillo, M. P.; Szpikowska, B. K.; Mas, M. T.; Sutin, J. D.; Beechem, J. M. Real-Time Measurement of Multiple Intramolecular Distances During Protein Folding Reactions: A Multisite Stopped-Flow Fluorescence Energy-Transfer Study of Yeast Phosphoglycerate Kinase. *Biochemistry* **1997**, *36*, 11273–11281.
7. Ha, T.; Enderle, T.; Ogletree, D. F.; Chemla, D. S.; Selvin, P. R.; Weiss, S. Probing the Interaction between Two Single Molecules: Fluorescence Resonance Energy Transfer between a Single Donor and a Single Acceptor. *Proc. Natl. Acad. Sci. U.S.A.* **1996**, *93*, 6264–6268.
8. Selvin, P. R. Principles and Biophysical Applications of Lanthanide-Based Probes. *Annu. Rev. Biophys. Biomol. Struct.* **2002**, *31*, 275–302.
9. Charbonnière, L. J.; Hildebrandt, N. Lanthanide Complexes and Quantum Dots: A Bright Wedding for Resonance Energy Transfer. *Eur. J. Inorg. Chem.* **2008**, *2008*, 3241–3251.
10. Sueda, S.; Yuan, J. L.; Matsumoto, K. A Homogeneous DNA Hybridization System by Using a New Luminescence Terbium Chelate. *Bioconjugate Chem.* **2002**, *13*, 200–205.
11. Song, B.; Wang, G. L.; Tan, M. Q.; Yuan, J. L. A Europium(III) Complex as an Efficient Singlet Oxygen Luminescence Probe. *J. Am. Chem. Soc.* **2006**, *128*, 13442–13450.
12. Selvin, P. R.; Hearst, J. E. Luminescence Energy Transfer Using a Terbium Chelate: Improvements on Fluorescence Energy Transfer. *Proc. Natl. Acad. Sci. U.S.A.* **1994**, *91*, 10024–10028.
13. Mathis, G. Rare Earth Cryptates and Homogeneous Fluoroimmunoassays with Human Sera. *Clin. Chem.* **1993**, *39*, 1953–1959.
14. Mathis, G. Probing Molecular-Interactions with Homogeneous Techniques Based on Rare-Earth Cryptates and Fluorescence Energy-Transfer. *Clin. Chem.* **1995**, *41*, 1391–1397.
15. Mathis, G.; Socquet, F.; Viguier, M.; Darbouret, B. Homogeneous Immunoassays Using Rare Earth Cryptates and Time Resolved Fluorescence: Principles and Specific Advantages for Tumor Markers. *Anticancer Res.* **1997**, *17*, 3011–3014.
16. Cummings, R. T.; McGovern, H. M.; Zheng, S.; Park, Y. W.; Hermes, J. D. Use of a Phosphotyrosine−Antibody Pair as a General Detection Method in Homogeneous Time-Resolved Fluorescence: Application to Human Immunodeficiency Viral Protease. *Anal. Biochem.* **1999**, *269*, 79–93.
17. Stenroos, K.; Hurskainen, P.; Eriksson, S.; Hemmilä, I.; Blomberg, K.; Lindqvist, C. Homogeneous Time-Resolved IL-2-IL-2R Alpha Assay Using Fluorescence Resonance Energy Transfer. *Cytokine* **1998**, *10*, 495–499.
18. Blomberg, K.; Hurskainen, P.; Hemmilä, I. Terbium and Rhodamine as Labels in a Homogeneous Time-Resolved Fluorometric Energy Transfer Assay of the Beta Subunit of Human Chorionic Gonadotropin in Serum. *Clin. Chem.* **1999**, *45*, 855–861.
19. Karvinen, J.; Laitala, V.; Makinen, M. L.; Mulari, O.; Tamminen, J.; Hermonen, J.; Hurskainen, P.; Hemmila, I. Fluorescence Quenching-Based Assays for Hydrolyzing Enzymes. Application of Time-Resolved Fluorometry in Assays for Caspase, Helicase, and Phosphatase. *Anal. Chem.* **2004**, *76*, 1429–1436.
20. Tsourkas, A.; Behlke, M. A.; Xu, Y. Q.; Bao, G. Spectroscopic Features of Dual Fluorescence/Luminescence Resonance Energy-Transfer Molecular Beacons. *Anal. Chem.* **2003**, *75*, 3697–3703.
21. Posson, D. J.; Ge, P. H.; Miller, C.; Bezanilla, F.; Selvin, P. R. Small Vertical Movement of a K1 Channel Voltage Sensor Measured with Luminescence Energy Transfer. *Nature* **2005**, *436*, 848–851.
22. Lessard-Viger, M.; Rioux, M.; Rainville, L.; Boudreau, D. FRET Enhancement in Multilayer Core−Shell Nanoparticles. *Nano Lett.* **2009**, *9*, 3066–3071.
23. Wang, L.; Tan, W. Multicolor FRET Silica Nanoparticles by Single Wavelength Excitation. *Nano Lett.* **2006**, *6*, 84–88.
24. Caruso, F. Nanoengineering of Particle Surfaces. *Adv. Mater.* **2001**, *13*, 11–22.
25. Ai, K. L.; Zhang, B. H.; Lu, L. H. Europium-Based Fluorescence Nanoparticle Sensor for Rapid and Ultrasensitive Detection of an Anthrax Biomarker. *Angew. Chem., Int. Ed.* **2009**, *48*, 304–308.
26. Wang, F.; Liu, X. G. Recent Advances in the Chemistry of Lanthanide-Doped Upconversion Nanocrystals. *Chem. Soc. Rev.* **2009**, *38*, 976–989.

27. Ma, Y.; Wang, Y. Recent Advances in the Sensitized Luminescence of Organic Europium Complexes. *Coord. Chem. Rev.* **2010**, *254*, 972–990.
28. Ferrand, A. C.; Imbert, D.; Chauvin, A. S.; Vandevyver, C. D. B.; Bunzli, J. C. G. Non-cytotoxic, Bifunctional $Eu^{III}$ and $Tb^{III}$ Luminescent Macrocyclic Complexes for Luminescence Resonant Energy-Transfer Experiments. *Chem.—Eur. J.* **2007**, *13*, 8678–8687.
29. Gu, J. Q.; Shen, J.; Sun, L. D.; Yan, C. H. Resonance Energy Transfer in Steady-State and Time-Decay Fluoro-Immunoassays for Lanthanide Nanoparticles Based on Biotin and Avidin Affinity. *J. Phys. Chem. C* **2008**, *112*, 6589–6593.
30. Gu, J. Q.; Sun, L. D.; Yan, Z. G.; Yan, C. Luminescence Resonance Energy Transfer Sensors Based on the Assemblies of Oppositely Charged Lanthanide/Gold Nanoparticles in Aqueous Solution. *Chem. Asian J.* **2008**, *3*, 1857–1864.
31. Santra, S.; Zhang, P.; Wang, K.; Tapec, R.; Tan, W. Conjugation of Biomolecules with Luminophore-Doped Silica Nanoparticles for Photostable Biomarkers. *Anal. Chem.* **2001**, *73*, 4988–4993.
32. Tan, M. Q.; Ye, Z. Q.; Wang, G. L.; Yuan, J. L. Development of Functionalized Fluorescent Europium Nanoparticles for Biolabeling and Time-Resolved Fluorometric Applications. *J. Mater. Chem.* **2004**, *14*, 2896–2901.
33. Song, C. H.; Ye, Z. Q.; Wang, G. L.; Jin, D. Y.; Yuan, J. L.; Guan, Y. F.; Piper, J. Preparation and Time-Gated Luminescence Bioimaging Application of Ruthenium Complex Covalently Bound Silica Nanoparticles. *Talanta* **2009**, *79*, 103–108.
34. Zhang, H.; Xu, Y.; Yang, W.; Li, Q. G. Dual-Lanthanide-Chelated Silica Nanoparticles as Labels for Highly Sensitive Time-Resolved Fluorometry. *Chem. Mater.* **2007**, *19*, 5875–5881.
35. Jiang, H. F.; Wang, G. L.; Zhang, W. Z.; Liu, X. Y.; Ye, Z. Q.; Jin, D. Y.; Yuan, J. L.; Liu, Z. G. Preparation and Time-Resolved Luminescence Bioassay Application of Multicolor Luminescent Lanthanide Nanoparticles. *J. Fluoresc.* **2010**, *20*, 321–328.
36. Latva, M.; Takalo, H.; Mukkala, V. M.; Matachescu, C.; Rodríguez-Ubis, J. C.; Kankare, J. Correlation between the Lowest Triplet State Energy Level of the Ligand and Lanthanide(III) Luminescence Quantum Yield. *J. Lumin.* **1997**, *75*, 149–169.
37. Vetrone, F.; Naccache, R.; Mahalingam, V.; Morgan, C. G.; Capobianco, J. A. The Active-Core/Active-Shell Approach: A Strategy To Enhance the Upconversion Luminescence in Lanthanide-Doped Nanoparticles. *Adv. Funct. Mater.* **2009**, *19*, 2924–2929.
38. Haldar, K. K.; Sen, T.; Patra, A. Au@ZnO Core−Shell Nanoparticles Are Efficient Energy Acceptors with Organic Dye Donors. *J. Phys. Chem. C* **2008**, *112*, 11650–11656.